Green Chemistry

PAPER

View Article Online
View Journal | View Issue

Cite this: *Green Chem.*, 2025, **27**, 12642

Sustainable upcycling of polyethylene waste to compatibilizers and valuable chemicals

Darien K. Nguyen, †[a,b] Zoé O. G. Schyns, †[a,b] LaShanda T. J. Korley *[a,b,c] and Dionisios G. Vlachos *[a,b]

Received 3rd June 2025,
Accepted 8th September 2025

DOI: 10.1039/d5gc02799c

rsc.li/greenchem

Controllable functionalization of polyethylene (PE) waste could generate new polymeric materials that are generally difficult to manufacture sustainably while also addressing the growing plastics waste problem. However, these modifications remain challenging due to the inherent stability of the PE backbone. Non-thermal atmospheric plasma enables molecular activation under mild conditions while utilizing renewable energy but is primarily employed for surface modification, as plasmas do not penetrate the bulk of materials. Herein, controllable bulk oxidative functionalization of PE wax (PEW) and low-density PE (LDPE) of varying molecular weights was achieved, with up to 6 mol% oxygen incorporation, by manipulating melt viscosity. This functionalization was accomplished either through temperature adjustment or by introducing a melt viscosity modifier, removable *via* simple extraction methods, to reduce LDPE viscosity, enhance diffusion and chain mobility, and enable bulk oxidation. The oxidized LDPE induces compatibilization in blends of poly(lactic acid) (PLA) and LDPE with improved interfacial adhesion and mechanical properties, such as a 70% increase in elongation-at-break values *vs.* the control. These findings pave the way for catalyst-free upcycling of direct plastics waste and plastics waste-derived products, enabling the creation of high-value products across various markets.

Green foundation

1. This manuscript presents a fully electrified, catalyst-free approach to upcycle plastics waste (polyethylene {PE} and PE-derived products) *via* oxyfunctionalization into new materials for high-value markets. Current functionalization strategies for these polymers rely on complex catalysts, strong oxidants, solvents, high temperatures, and long treatment times, which heighten environmental impact and raise sustainability concerns.
2. Overall, this work presents an effective one-step, post-polymerization functionalization method that overcomes existing energetic barriers to PE functionalization. Our electrification approach upcycles plastics waste into enhanced compatibilizers, facilitating the adhesion of incompatible polymers to create products with superior mechanical properties.
3. This work could be strengthened by further research into plasma chemistry for the activation of bulk polymers. It would also benefit from direct comparisons with conventional polymer oxidation methods.

Introduction

The steady increase in global plastics production over the past few decades, coupled with the linearity of the current plastics lifecycle, has resulted in pervasive and ubiquitous plastics pollution.[1–3] By the end of 2017, over seven billion tons of plastics waste were generated.[3] Of this accumulated plastics waste, only 10% was recycled—*via* primarily mechanical means (*i.e.*, plastics extrusion)—during which the heat and shear forces degrade polymer physical properties.[2] Around 14% was incinerated for energy recovery (heat and electricity), offering a considerable reduction in waste volume while bypassing waste sorting and separation steps.[4,5] However, such processes are not circular and can result in air pollution (particulate matter), greenhouse gas emissions, and toxic byproducts (heavy metals, dioxins, ash waste).[1,4–6] The remaining 76% ended up in landfills, dumps, or the natural environment, raising significant environmental and health concerns.[1,7,8] Consequently, there is an urgent need to curb environmental pollution and landfilling rates by developing more circular waste management strategies. One route toward improved materials circularity is upcycling, in which waste materials are

[a]*Department of Chemical and Biomolecular Engineering, University of Delaware, Newark, Delaware 19716, USA. E-mail: lkorley@udel.edu, vlachos@udel.edu*
[b]*Center for Plastics Innovation, University of Delaware, Newark, Delaware 19716, USA*
[c]*Department of Materials Science Engineering, University of Delaware, Newark, Delaware 19716, USA*
†Contributed equally.

chemically or otherwise modified into new, valuable materials and chemicals.[9]

Functionalized polyethylene (PE) and polyethylene wax (PEW), specifically oxidized PE and PEW, are increasingly sought after for their diverse applications in plastics processing, paints, coatings, and printing inks.[10] The insertion of oxygen-containing functional groups along the polymer chain can significantly alter their properties.[11–13] This functionalization approach can enhance adhesive strength and compatibilization by increasing the number and strength of interactions across interfaces.[11–13] Compatibilization of immiscible polymers offers a strategy to address issues associated with plastic contamination and sorting, which are significant barriers to producing high-quality, mechanically recycled plastics. By improving interfacial adhesion and phase dispersion of mixed polymers, compatibilization can enhance the mechanical performance and durability of mechanically recycled plastics, supporting circularity in plastic waste management.[11,14]

Functionalizing PE and PEW into value-added materials is challenging due to the stability of their homo-atom backbones.[13] Oxidized PEs and PEWs are typically manufactured *via* organic syntheses. Oxidized PEWs are normally made by a two-step process comprised of catalytic thermal decomposition of PEs followed by oxidation under high temperatures (>140 °C) and pressures (>1 atm) using various catalysts (*e.g.*, $KMnO_4$).[10] The oxidative functionalization of PEs, on the other hand, is less explored, as functionalized polymers, in general, are typically synthesized *via* copolymerization of ethylene with specialized monomers (*e.g.*, acrylic acid, vinyl alcohol, ethylene oxide).[15–19] While highly successful, copolymerization is often hampered by catalyst poisoning caused by the polarity of the new functional groups.[16] Additional reagents and process steps are typically required to protect these functional groups during polymerization and de-protect them afterward. Controlling functional group incorporation remains difficult in copolymerization due to different relative rates of monomer polymerization.[16] Post-polymerization functionalization of waste plastics could extend end-of-life use and facilitate circularity,[20] presenting as a more attractive approach. Current post-polymerization functionalization methods[20] have proven as effective oxidative upcycling tactics,[21] but typically require complex metal catalysts (metal complexes and metalloenzymes), strong oxidants (acids, *etc.*), solvents (dichloroethane, *etc.*), high temperatures (>120 °C), and long treatment times, which increase environmental impacts and raise sustainability concerns.[22] Other common routes to achieve PE functionalization include solution- or extruder-based peroxide-initiated functionalization; yet these approaches necessitate the use of peroxides (dicumyl peroxide, benzolyl peroxide, *etc.*),[23] which present additional safety challenges due to their sensitivity to heat and decomposition into explosive compounds.[24] The use of peroxides for C–H activation also can negatively impact the properties of the polymer by inducing β-scission and reducing the polymer's overall molecular weight.[23,25] Additionally, this type of functionalization typically requires one or more—depending upon final chemical requirements—functionalization agents, which can increase process costs.[25,26] Finding a sustainable approach for directly and controllably functionalizing waxes and polymers with limited addition of chemicals can be game-changing for producing valuable products from plastic waste.

Non-thermal atmospheric plasma (NTAP) is an electrified, green chemical manufacturing technology capable of molecular activation at ambient conditions[27–30] through collisions of energetic electrons with gas molecules, generating ions, free radicals, and excited species.[28,31,32] Oxidative plasma has been extensively applied in rapidly functionalizing polymer and carbon surfaces.[28,33–35] Yet, this functionalization strategy is typically limited to the surface of the polymer[34,35] due to the plasma's inability to penetrate non-porous materials, resulting in reactions at the plasma/polymer interface. For solid polymers and substrates, the thickness of the reported affected layer ranges from a few nanometers to microns depending on the various plasma parameters, reactor designs, and substrate materials.[35–37] Consequently, bulk functionalization of polymers using NTAP has yet to be demonstrated.

This study presents a novel, controlled, bulk oxidative functionalization of solid PEWs, which can be produced *via* hydrogenolysis of PEs, and higher molecular weight, low-density PEs (LDPEs) using oxygen-based NTAP. This approach requires no functionalization agents or initiators, unlike existing routes to oxidized PEs. PEWs were plasma oxidized comparably to commercially available oxidized waxes, by tuning the process conditions. The oxidized waxes exhibited lower melting points, crystallinities, and molecular weights, but enhanced thermal stability, indicating an interplay between chain oxidation, scission, and cross-linking reactions. Plasma oxidation of waste-comparable, molten LDPEs under the same conditions was unsuccessful due to the high viscosity of the melt. Using PE hydrogenolysis-like products, we engineered the melts to achieve bulk oxidation of high molecular weight LDPEs through a viscosity modifier approach by reducing the overall viscosity of the melt. This viscosity modifier can be easily removed from the oxidized LDPE by simple extraction methods. Importantly, the oxidized PEs are excellent compatibilizers in LDPE/poly(lactic acid) (PLA) polymer blends, taken as an example immiscible system, enhancing phase interactions and mechanical properties. Overall, this work introduces an effective one-step, post-polymerization functionalization method, bypassing the barriers to PE functionalization. This electrification approach can upcycle plastic waste to enhanced compatibilizers for adhering incompatible polymers into products with improved mechanical properties. Additionally, this approach can utilize plastic waste-derived hydrogenolysis products, such as waxes, for chemical applications in plastics processing, paints, coatings, and printing inks.

Results and discussion

Plasma oxidation was initially performed on the PEW by melting the wax (>110 °C) and impinging the oxygen plasma

on the surface of the melt (Fig. 1a). Operating at these higher temperatures reduces the viscosity of PEW and increases chain mobility and diffusion of oxygenated groups, enabling bulk oxyfunctionalization. Oxygen incorporation in the polymer wax was studied using X-ray photoelectron spectroscopy (XPS), Fourier-transform infrared (FTIR) spectroscopy, and variable-temperature ^{1}H nuclear magnetic resonance (NMR) spectroscopy (Fig. 1b–d). XPS determined the atomic percentage of oxygen species on the resolidified PEW surface (Fig. 1b). XPS survey spectra used to calculate oxygen atomic percentages are shown in Fig. S5. Longer plasma treatment times increased the oxygen incorporation, reaching up to ~6% after 4 h. The FTIR spectra confirmed the presence of carbonyl and hydroxyl groups (Fig. 1c). A sharp peak at 1720 cm^{-1} and a broad peak around 1000–1200 cm^{-1} were attributed to C=O stretching and C–O stretching vibrations, respectively. Additionally, a broad peak at 3400 cm^{-1} and a sharp peak at 1410 cm^{-1} were assigned to O–H stretching.[38] The relative intensity of these peaks increased, compared to CH_2 symmetric and asymmetric stretches at ~2850 and ~2920 cm^{-1}, with longer plasma treatments, indicating higher oxygen content. The characteristic peaks of C–H bonds in methyl and methylene groups were dominant in all FTIR spectra (Fig. 1c). While FTIR and XPS could be utilized to examine both bulk and homogeneous oxidation by analyzing different faces of molten PEW (mid-plane and opposite), removal from the reactor vial and processing of the molten PEW proved difficult. Therefore, to provide evidence of homogeneous oxidation through the melt, submicron IR spectroscopy (mIRage) measurements on the cross-section of the molten PEW were performed. Spectra showed clear C=O stretching (1720 cm^{-1}) and C–H bending (1470 cm^{-1}) consistently across the cross-section, confirming uniform oxidation throughout the melt (Fig. S6). To validate the bulk functionalization of the PEW in a more accurate, quantitative approach, ^{1}H NMR was conducted on dissolved samples (1,1,2,2 tetrachloroethane-d_2) (Fig. 1d and Fig. S3). Peaks corresponding to carbonyl (δ 2.4 ppm), hydroxyl (δ 3.6 ppm and 3.9 ppm), aldehyde (δ 9.8 ppm), and alkene (δ 5.5 ppm) groups emerged in NMR spectra at increasing treatment times. The dual hydroxyl peaks were due to primary (δ 3.9 ppm) and secondary alcohols (δ 3.6 ppm). By integrating the peaks relative to the methyl and methylene groups (δ 1.8–0.6 ppm), the functional group incorporation into the polymer chain (mol%) was calculated [see Materials & methods, Fig. S3, and eqn (S1), (S2)]. Gravimetric, gas trap, and output stream analysis indicated negligible formation of exiting gas-phase hydrocarbons (Fig. S7). These results demonstrate that NTAP can achieve bulk oxidation of low molecular weight polymers, such as PEWs, through the plasma-melt interface, a process that has not been shown previously.

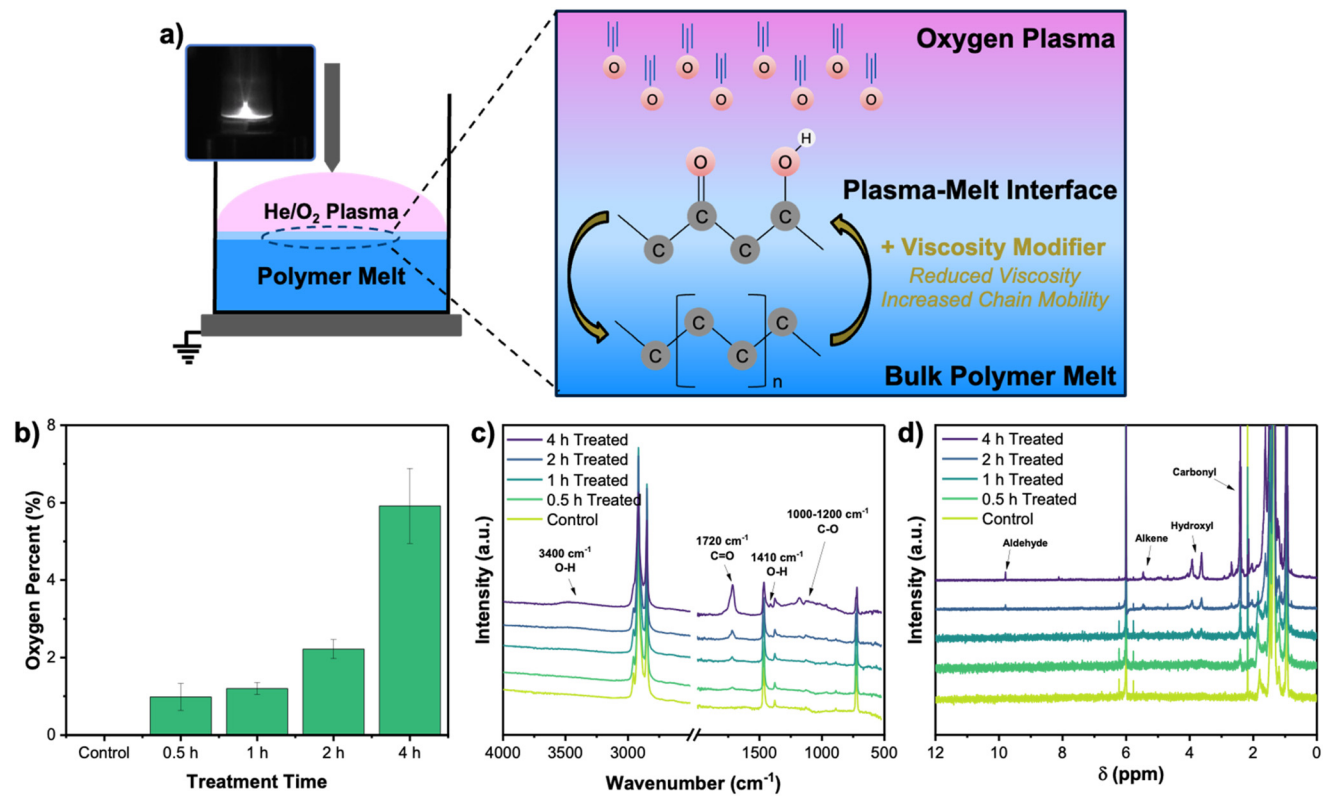

Fig. 1 (a) Schematic of the plasma–melt interface in the pin-to-plate reactor with iCCD image of pulsed discharge. (b) XPS atomic percentages, (c) FTIR spectra, and (d) ^{1}H NMR spectra of neat and plasma-treated PEW at various treatment times. Plasma operating conditions: O_2 feed molar percent: 1%, stir rate: 0 rpm, and temperature: 110 °C. XPS conditions: survey scan at 20 eV and 100 ms dwell time. FTIR conditions: MCTB detector at 4.0 cm^{-1} resolution and 32 scans. ^{1}H NMR conditions: 115 °C in 1,1,2,2-tetrachloroethane-d_2.

Fig. S8 depicts a reaction scheme for the oxidation of PEW or molten PE using oxygen-rich plasma chemistry based on the product distribution and previous literature,[30,39–42] where the molten PE behaves similarly to liquid alkanes. The reaction is initiated by the hydrogen abstraction of the polymer chain by reactive oxygen species (O^3P).[30,40,42] Through recombination with abundant oxygen species, alkyl radicals form hydroxyl and peroxide groups. The hydroperoxide species are relatively unstable and readily dissociate into hydroxyl and carbonyl-containing species (*i.e.*, aldehydes and ketones).[43] Hydroxyl groups can also undergo oxidation to the corresponding aldehydes or ketones. Additionally, carbons connected with hydroxyl or aldehyde groups can undergo carbon–carbon cleavage, leading to chain scission. Consecutive hydrogen abstractions on a polymer chain can create multiple alkyl radicals, yielding alkene functional groups. Termination reactions between alkyl radicals can potentially lead to polymer crosslinking.[39,40]

Presented in Fig. 2 is the effect of treatment time, O_2 feed molar fraction, stir rate, and temperature on the oxidation of the PEW. All functional groups were quantified using ^{1}H NMR analysis (Materials and methods). Increasing treatment time led to greater oxygen functionality in the polymer chain due to longer residence times of the melt within the plasma reactor (Fig. 2a). The calculated oxygen incorporation from ^{1}H NMR showed similar trends to the atomic oxygen percentage calculated by XPS (Fig. 1a), indicating relatively uniform oxidation throughout the melt. Differences between XPS and NMR data can be associated with XPS being an extremely surface-sensitive technique and adsorbed O_2 from air (or plasma) on the surface of the PEW can cause variability.[44] Higher O_2 feed molar percentages initially led to higher oxygen incorporation, but functionalization plateaued at 4% O_2 feed (Fig. 2b). This plateau occurred because higher oxygen feed percentages lead to decreasing dissipated power at fixed applied voltages and frequencies.[39] Additionally, the electronegative nature of O_2 reduces the electron density of the plasma, resulting in reduced generation of reactive oxygen species.[39] Modifying the stirring rate from 0 to 300 rpm (Fig. 2c) revealed minimal differences in oxidation, which we attribute to the natural convection induced by the plasma impingement on the melt surface dominating PEW flow. Increasing the melt temperature from 110 to 170 °C (Fig. 2d) increased oxidation from 0.4 to 0.9 mol% respectively, potentially due to (1) an increase in the

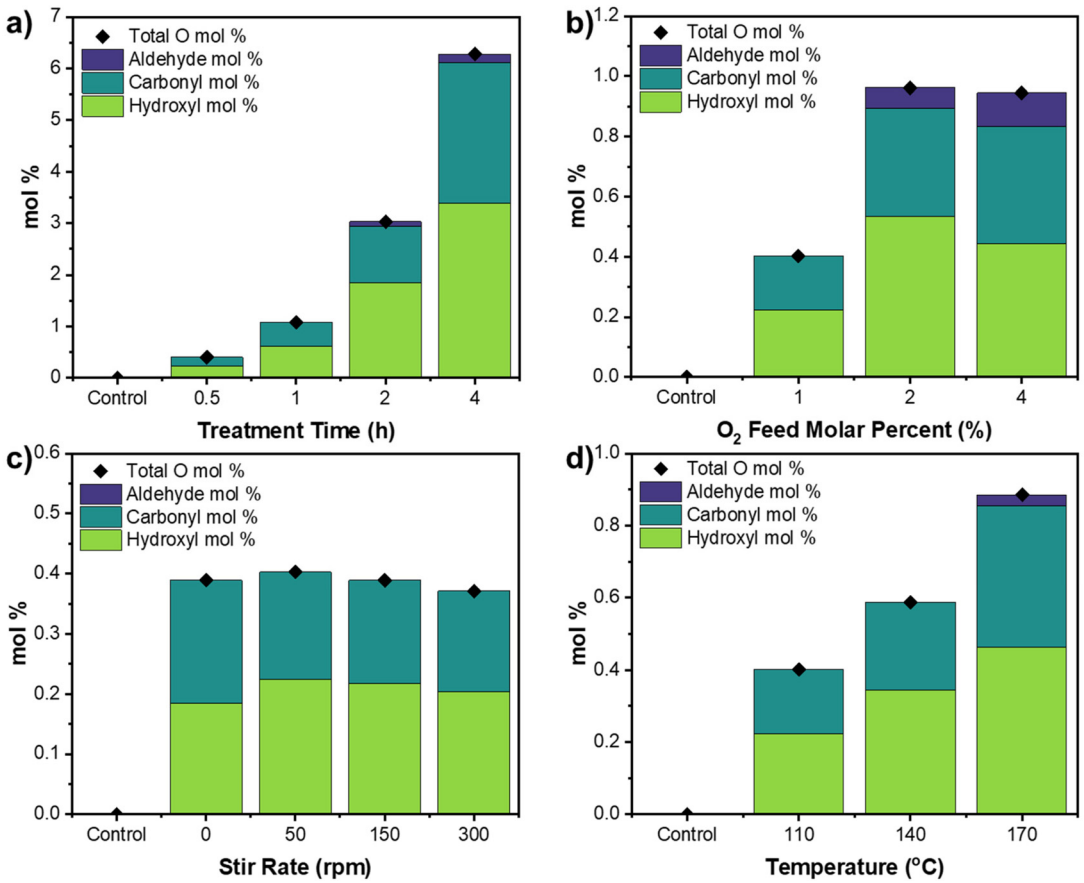

Fig. 2 Oxygen percentages and type of functional group incorporation for neat and plasma-oxidized PEW at varying (a) treatment times, (b) O_2 feed molar percents, (c) stirring rates, and (d) temperatures. Carbonyl groups refer to middle chain C=O bonds while aldehyde groups refer to end chain C=O groups. Quantification from ^{1}H NMR performed at 115 °C in 1,1,2,2-tetrachloroethane-d_2. Plasma operating conditions (unless otherwise specified): treatment time: 0.5 h, O_2 feed molar percent: 2%, stir rate: 0 rpm, and temperature: 110 °C.

vapor pressure of the melt,[39] which allows for more gas-phase interactions, or (2) a decrease in the melt viscosity (Fig. S9), facilitating the diffusion of oxygen groups into the melt and the counter diffusion of functionalized and bulk polymer chains.[45] Alcohol and carbonyl groups were in almost equal ratios at low oxygen incorporation. However, at higher oxidation intensities (*i.e.*, higher O_2 inputs or longer treatment times), aldehyde groups became increasingly prevalent. This change in functionalization may result from further oxidation of alcohol groups or from carbon cleavage forming smaller-chain aldehydes. Overall, these results demonstrate that NTAP can controllably oxidize low molecular weight polymers (*i.e.*, PEWs) purely in the melt phase by optimizing process conditions.

Differential scanning calorimetry (DSC), thermogravimetric analysis (TGA), and high-temperature gel permeation chromatography (HT-GPC) analysis (Fig. 3) indicated several changes in PEW properties post-plasma treatment. DSC curves from second heating (Fig. 3a) revealed that the control PEW has a melting point of ~75 °C, which decreases with longer treatment times (*i.e.*, higher oxidation). Additionally, the melting peak broadened and decreased in intensity. By calculating and comparing the melting enthalpy to that of a perfect PE crystal, the crystallinity of the final product can be determined[46] [eqn (2), Fig. S10, and Table S1]. At higher treatment times, the crystallinity and melting point of the treated PEWs decreased, which may be due to the introduction of oxygen groups along the backbone disrupting the packing of polymer chains during crystallization. Additionally, crosslinking of the polymer chain and/or a decrease in the molecular weight of the polymer due to carbon cleavage can reduce crystallinity and melting temperature,[47,48] both of which can occur at the plasma-melt interface. These competing effects are further revealed in TGA traces of the polymer before and after plasma treatment (Fig. 3b), which indicates a higher decomposition temperature onset for the plasma-oxidized PEW compared to neat PEW. The peak of the first derivative of the TGA weight loss curve was approximately 310 °C for the control PEW and 340 °C for the plasma-treated PEW (Fig. S11), indicating that the most significant weight loss changes occurred at higher temperatures in the plasma-treated samples. This increased thermal stability could be tentatively attributed to the crosslinking of

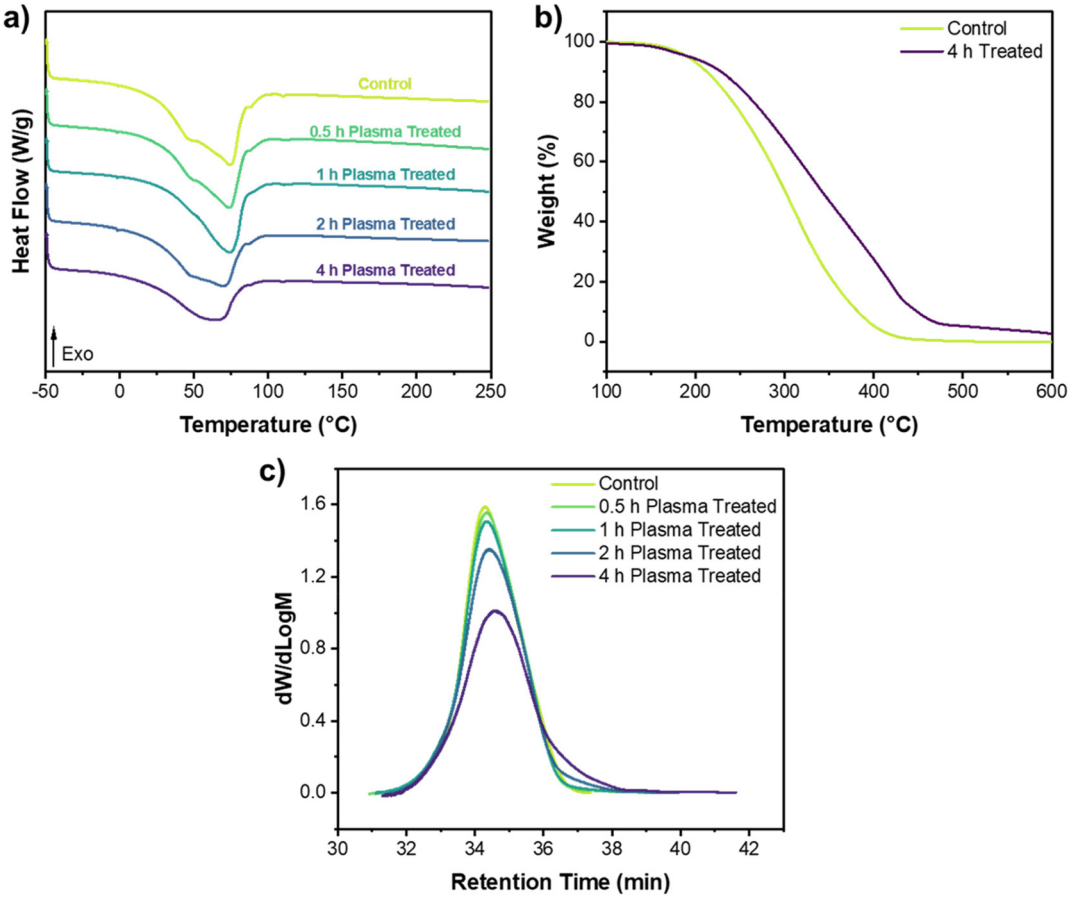

Fig. 3 (a) DSC, (b) TGA, and (c) HT-GPC traces of neat and plasma-oxidized PEW at varying treatment times. Plasma operating conditions: O_2 feed molar percent: 1%, stir rate: 0 rpm, and temperature: 110 °C. DSC conditions: ramps of 10 °C min^{-1} from −50 °C to 200 °C. DSC curves are from 2nd heating curve, plotted exotherm up and arbitrarily shifted to compare peaks. TGA conditions: ramp 10 °C min^{-1} from 100–600 °C under N_2 gas. HT-GPC: conducted in 1,2,4-trichlorobenzene and calibrated against polystyrene standards.

the polymer chain, which aligns with the DSC analysis, resulting in a polymer with slightly enhanced thermal stability (further discussed for NTAP of LDPE below). However, molecular weight distributions (MWD) from HT-GPC analysis showed broadening at longer plasma treatment times, accompanied by a shift toward higher retention times, indicating a slight decrease in the molecular weight due to oxidative carbon cleavage. As previously stated, both crosslinking and carbon cleavage reactions may occur simultaneously, but HT-GPC omits testing of cross-linked insoluble fractions of the sample. Therefore, the changes to the polymer architecture are complex, with a likely interplay between crosslinking and chain scission during plasma oxidation.

The acid number and oxygen mol% of plasma-oxidized PEW were compared to commercially available oxidized waxes of Deurex (Fig. 4). The Deurex oxidized waxes (commercially named LDPE EO 75K and 78K) were obtained as representatives of commercially available, highly and lightly oxidized PEWs, with molecular weights expected to be similar to that of neat PEW. Higher acid numbers are typically characterized by greater oxidation of the polymer chain, as the acid number represents the milligrams of KOH needed to neutralize per gram of polymer. NTAP achieved acid numbers comparable to commercial oxidized waxes produced conventionally (*i.e.*, at high pressures and temperatures), even under unoptimized conditions (Fig. 4a). Plasma oxidation facilitates a larger diversity of functional groups than commercial waxes (Fig. 4b), with hydroxyl and carbonyl groups in near-equal ratios and a small number of aldehyde groups at higher oxidation levels. In contrast, commercial oxidized waxes predominantly contained carbonyl groups with a small fraction of hydroxyl groups. Overall, plasma treatment can achieve similar acid numbers to commercial waxes in a controllable manner while introducing a diverse array of functional groups. Further comparison of the thermal properties and molecular weights of plasma-oxidized and commercially oxidized waxes was conducted (Fig. S12). The commercially oxidized waxes exhibited substantially different molecular weights than the control PEW, suggesting their synthesis from a PEW of a higher starting molecular weight. To assess the potential replacement of current commercial processes with plasma processes, a more detailed comparison using an identical starting PEW is essential to isolate plasma effects and will be the subject of future work. Given the applicability of plasma functionalization over the spectrum of molecular weights (see below), functionalization of any molecular weight PEW should be feasible. Plasmas provide a viable alternative to produce oxidized PEWs for applications in plastics processing, paints, coatings, printing inks, *etc.*[10]

To showcase the functionalization of materials with molecular weights representative of LDPE products, LDPE (M_w ~40 kg mol^{-1}) was plasma treated. Bulk plasma oxidation of the neat LDPE proved challenging even >200 °C at the optimal conditions for PEW (Fig. S13). This challenge is attributed to the high viscosity of the molten LDPE (4.34 Pa s – Fig. S14), which could prevent the diffusion of the oxygen groups into the bulk and the counter diffusion of bulk melt.[45,49,50] Instead, the surface gets overoxidized, leading to gas-phase oxygenates manifested as mass loss (Fig. S15). Additionally, autoxidation and polymer degradation prevailed at high temperatures in the open air (*i.e.*, no plasma; Fig. S13). Therefore, to reduce the viscosity of the melt and the operating temperature, *n*-octacosane (*n*-C_{28}) was added to the melt at varying ratios (Fig. 5). Since *n*-C_{28} forms a homogeneous mixture with LDPE due to their chemical similarity, the addition of *n*-C_{28} should only affect the melt viscosity and should not have any other chemical or physical effects on the system. *n*-C_{28} was selected for its low vapor pressure to limit evaporation and gas-phase plasma reactions, similar oxidation to PEW, and simple extraction (*i.e.*, *via* hexanes and sonication). Importantly, long-chain alkanes are produced by mild hydrogenolysis of plastic waste, making the whole process sustainable and enabling plastic circularity.[39,40,51] The oxygen of

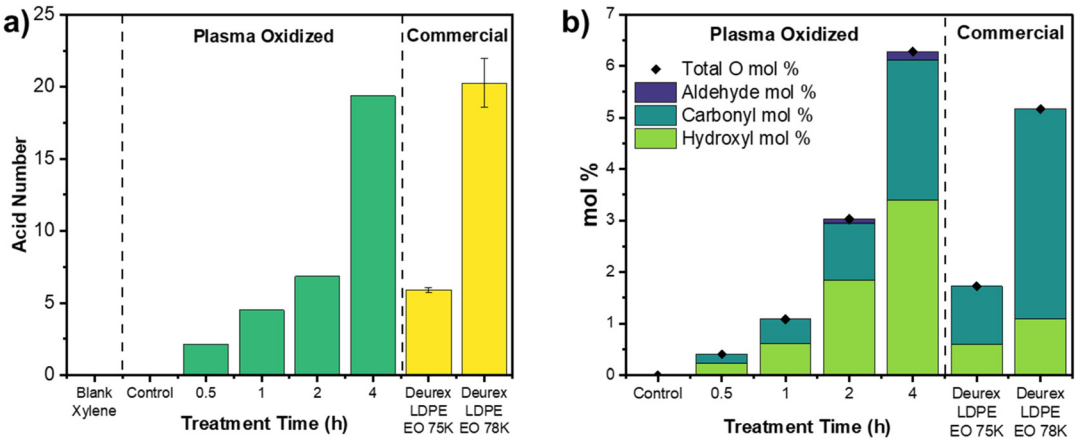

Fig. 4 (a) Acid number and (b) corresponding oxygen percentages and functional group incorporation of neat, plasma-treated, and commercially oxidized waxes. Carbonyl groups refer to middle chain C=O bonds while aldehyde groups refer to end chain C=O groups. Plasma operating conditions: O_2 feed molar percent: 1%, stir rate: 0 rpm, and temperature: 110 °C.

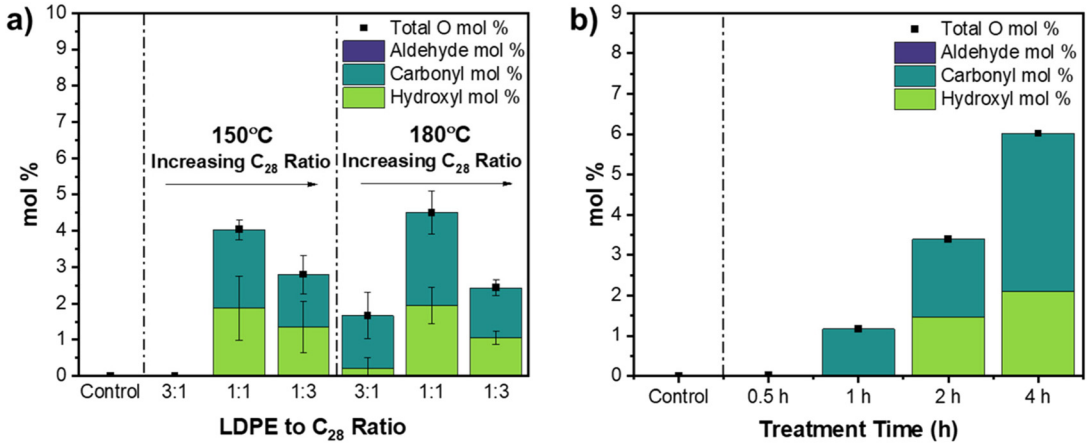

Fig. 5 Oxygen percentage and functional group incorporation in plasma-treated LDPE (40 kg mol^{-1}) at various (a) LDPE to C_{28} ratios at two temperatures and (b) treatment times at 150 °C and LDPE to C_{28} ratio of 1 : 1. The control (neat LDPE) is also shown. Carbonyl groups refer to middle chain C=O bonds while aldehyde groups refer to end chain C=O groups. Plasma operating conditions: treatment time: 2 h, O_2 feed molar percent: 2%, stir rate: 0 rpm.

NTAP-treated LDPE, after removal of *n*-C_{28} (discussed below), was estimated from the ^{1}H NMR spectra (Fig. S16) as previously described.

At 150 °C and 180 °C, maximum oxidation of LDPE was observed for an LDPE : C_{28} mixture with a ratio of 1 : 1, due to the mixture's viscosity and vapor pressure of C_{28}. Specifically, plasma oxidation of a 3 : 1 LDPE : C_{28} blend was limited by the high viscosity, especially at lower temperatures. Conversely, for a 1 : 3 LDPE : C_{28} blend, gas-phase C_{28} can compete for electron dissociation and decrease plasma intensity, lowering functionalization. Higher melt temperatures impact LDPE oxidation only slightly due to viscosity reduction. The temperature effect was most pronounced for 3 : 1 LDPE : C_{28}; no oxidation was observed at 150 °C *vs.* ~1% oxidation at 180 °C. The temperature effect became negligible at high fractions of C_{28} as the viscosity was sufficiently reduced. The tunability of functionalization was demonstrated by modulating the treatment time (Fig. 5). Up to 6 mol% oxidation of the polymer chain with simultaneous *n*-octacosane oxidation was achieved. Fig. S17 shows the conversion and yield of the *n*-octacosane products. These long-chain oxygenates can be used for the production of surfactants and lubricants.[39,40] To verify the hypothesis of the melt viscosity effect, the zero-shear (η_0) viscosities of the LPDE/C_{28} blends were estimated (Fig. S14b). Notably, the viscosity significantly dropped upon adding C_{28}; for example, at 150 °C, the viscosity decreased by ~4× (to 0.98 from 4.34 Pa s) upon adding 50 wt% C_{28} (Fig. S14). Increasing the temperature of the 1 : 1 LDPE : C_{28} blend decreased the viscosity from 0.98 Pa s at 150 °C to 0.08 Pa s at 180 °C (Fig. S13b). Therefore, as long as the melt viscosity is low enough to allow diffusion of oxygen groups and counter diffusion of bulk melt, this plasma technique is capable of treating any depth of molten polymer, limited only by reactor configuration. Overall, the addition of long-chain alkanes facilitates the plasma oxidation of LDPE by reducing the viscosity of the melt.

To highlight the broad applicability of this strategy, a higher molecular-weight LPDE (~76 kg mol^{-1}) was successfully oxidized at varying ratios (Fig. S18). Interestingly, higher oxidation was observed at a higher 1 : 3 LDPE : C_{28} ratio at 150 °C, attributed to the higher viscosity of the 76 kg mol^{-1} LDPE. This simple, variable fraction of hydrocarbon addition is an effective strategy that could potentially be extended to high-density PE (HDPE) (M_w ~10^2 kg mol^{-1})[52,53] or ultra-high molecular weight PE (M_w ~10^3 kg mol^{-1}),[54] which are otherwise difficult to functionalize in bulk due to their extremely high viscosity. While further research and optimization are needed to fully establish the viability of this plasma-based approach, these results are promising for generating a suite of functionalized materials from a variety of waste plastics.

The physical and thermal properties of the LDPE were assessed after plasma treatment (Fig. S19). As expected, the changes were similar to those observed in the plasma oxidation of PEWs. DSC traces indicated decreases in melting points and crystallinities [calculated according to eqn (4)], likely attributed to the introduction of oxygen groups, a reduction in the polymer molecular weight, and/or an increase in crosslinking.[55] Melting temperatures, enthalpies, and crystallinities are listed in Table S2. Akin to results observed for PEWs, TGA measurements indicated an increased thermal stability of the plasma-oxidized LDPE, which is attributed to the crosslinking of the polymer chains.[48] MWDs from HT-GPC indicated a minimal decrease in the molecular weight of LDPE by carbon cleavage (Fig. S19c). From Soxhlet extraction in xylenes, the degree of crosslinking of the plasma-treated LDPE increased with prolonged treatment time. Polymers treated for 2 h and 4 h had insoluble fractions (*i.e.*, gel contents) of 0.2% and 4.7%, respectively, compared to 0% for the neat LDPE control (Table S2). This mild increase in crosslinking *vs.* the control may contribute to the decrease in crystallinity;[55] however, deconvoluting the effects of oxidation, reduction

(from NMR, Fig. S3), crosslinking, and other chain modifications on the thermal properties of the LDPE remains difficult due to the complex reactions that occur during plasma treatment. These findings also indicate almost complete removal of n-C_{28} from the resulting oxidized LDPE by simple extraction methods, which would be evident in DSC and HT-GPC characterizations due to its low melting point (~61 °C) and molecular weight (M_w ~395 g mol^{-1}) compared to LDPE (110 °C, M_w ~40 kg mol^{-1}).

To test the plasma-oxidized LDPE as a polymer compatibilizer, non-polar LDPE (76 kg mol^{-1}) and polar PLA were melt-blended with 5 wt% neat LDPE (40 kg mol^{-1}) or 2 h plasma-oxidized LDPE (3.5 mol% oxygen incorporation, M_w ~40 kg mol^{-1}), as PLA and LDPE typically phase-separate with poor interfacial adhesion.[56] This PLA/LDPE blended system was selected for its well-documented immiscibility and the extensive range of compatibilization strategies available in the literature, making it an ideal choice for an initial proof-of-concept demonstration.[56–59] Scanning electron microscopy (SEM) imaging demonstrated the polymer blend morphology upon incorporating the compatibilizer. Fig. 6a–c shows SEM images of the LDPE/PLA blends containing 5 wt% of neat, non-oxidized LDPE; both samples displayed a droplet-in-matrix morphology (Fig. 6a–c). Clear phase separation was evident between PLA (secondary phase – circular droplets) and LDPE (primary phase – surrounding polymer matrix). Low magnification images (× 600 Fig. 6a) indicated a highly perforated cross-section of the polymer blend resulting from the distinct PLA and LDPE phases. Small voids between phases were manifested at closer magnifications (Fig. 6b and c) due to poor interfacial adhesion. Fig. 6d–f illustrates images upon adding the 5 wt% plasma-oxidized LDPE to the PLA/LDPE blend. At low magnification (Fig. 6d), a less perforated, more homogeneous cross-section was evident. Closer magnifications (Fig. 6e and f) indicate improved interfacial adhesion (compared to blends containing unfunctionalized LDPE), as the plasma-oxidized LDPE enhances interactions between PLA and LDPE due to polar and non-polar functional groups. We hypothesize that OH groups in the functionalized LDPE are hydrogen-bond donors, and C=O bonds in PLA are acceptors. Oxygen-rich regions in the treated LDPE enhance interfacial adhesion between the two phases.

TGA and DSC were conducted on PLA/LDPE blends (Fig. S20 and Table S3) to investigate the impact of the oxidized LDPE on the thermal properties of the blends. The glass transition temperature (T_g) of PLA (~55 °C) was determined from the 2nd heating DSC traces and remained unchanged in all PLA/LDPE blends (Table S3). Distinct T_gs indicate an immiscible, phase-separated blend, and the unchanged PLA T_g aligns with observations from SEM images (Fig. 6). The PLA control and the PLA-containing blend samples displayed bimodal endotherms corresponding to the melting of PLA crystalline domains at ~146 and ~150 °C (Fig. S20 and Table S3). This bimodal melting behavior is typically observed for PLA due to ordered and less ordered crystal structures (*e.g.*, α and α′ crystals) or differing crystal structures (*e.g.*, α, β, γ).[60,61] In some cases, bimodal endotherms in immiscible blends can result from morphological constraints of the semi-crystalline material[62] as interfaces can act as secondary nucleation sites;[62,63] however, the bimodal melting peak was also

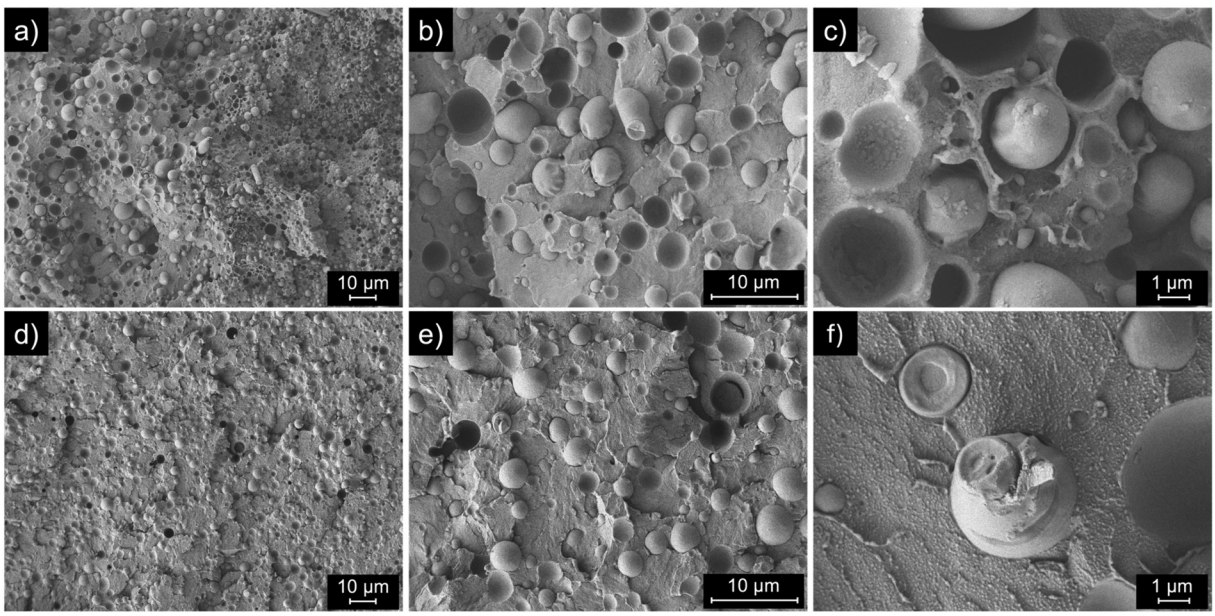

Fig. 6 SEM images of fractured (a–c) control polymer blend and (d–f) 5 wt% plasma-oxidized LDPE polymer blend. The polymer blend is 70% LDPE (76 kg mol^{-1}) and 30% PLA with the addition of 5 wt% neat LDPE (40 kg mol^{-1}) acting as the control or plasma-oxidized LDPE (3.5%, oxygen incorporation, 40 kg mol^{-1}) acting as a compatibilizer. Plasma operating conditions for plasma-oxidized LDPE: treatment time: 2 h, O_2 feed molar percent: 2%, stir rate: 0 rpm, temperature: 150 °C, and LDPE to C_{28} ratio of 1 : 1.

observed in the PLA control sample. A slight suppression in LDPE melting temperature (from 112 °C for neat LDPE to 109–110 °C for the blends) was seen upon inclusion of the lower molecular weight LDPE (40 kg mol^{-1}) as expected[64] (Fig. S20 and Table S3).

The crystallinity of the PLA phase decreased in blended samples relative to neat PLA (23.7% for the control and 23.3% for the oxidized-LDPE-containing sample *vs.* 33.3% in neat PLA) (Table S3). This behavior was similar for the LDPE crystallinity (32.9% for the control and 29.9% for the oxidized-LDPE-containing sample *vs.* 35.0% in neat LDPE) (Table S3). The mild decrease in crystallinity of the blends *vs.* the neat polymers can be explained by the interface between phases.[65] The interface or enhanced interfacial interactions can disrupt the crystalline packing of each polymer by hindering chain mobility or nucleation, ultimately suppressing the overall crystallinity.[65,66] The slightly lower crystallinity in the oxidized-PE-containing sample (*vs.* the non-oxidized-PE-containing sample) could be indicative of an increase in the quantity or nature of interfacial interactions (Fig. 6) or the lower crystallinity of the oxidized LDPE used (0.2% gel content, Table S2). Investigating the crystal structure and crystallization kinetics across varying PLA/LDPE/compatibilizer ratios could be leveraged to elucidate these complex interfacial phenomena further.

All blends exhibited similar thermal stability as revealed by TGA analyses (Fig. S20). A two-stage degradation process was observed for all samples, corresponding first to the degradation of PLA followed by that of LDPE. Additionally, the plasma-oxidized, compatibilized PLA/LDPE blends showed slightly higher thermal stability compared to the control, which could be due to crosslinking in the LDPE (0.2% gel content, Table S2) or enhanced interactions from compatibilization of the blend.[67]

Tensile testing of the PLA/LDPE blends was conducted to assess mechanical behavior with or without the incorporation of the plasma-oxidized LDPE (Fig. 7). Typically, the mechanics of an immiscible blended system are governed by the interphase quality and its ability to dissipate stress and prevent crack propagation through appropriate stress transfer.[68] For example, well-dispersed, small secondary phases have superior stress-transfer abilities relative to those with larger secondary phases, which can act as stress concentrators.[69] Additionally, voids created by poor interfacial adhesion or contact minimize stress transfer and result in inferior mechanical properties.[50]

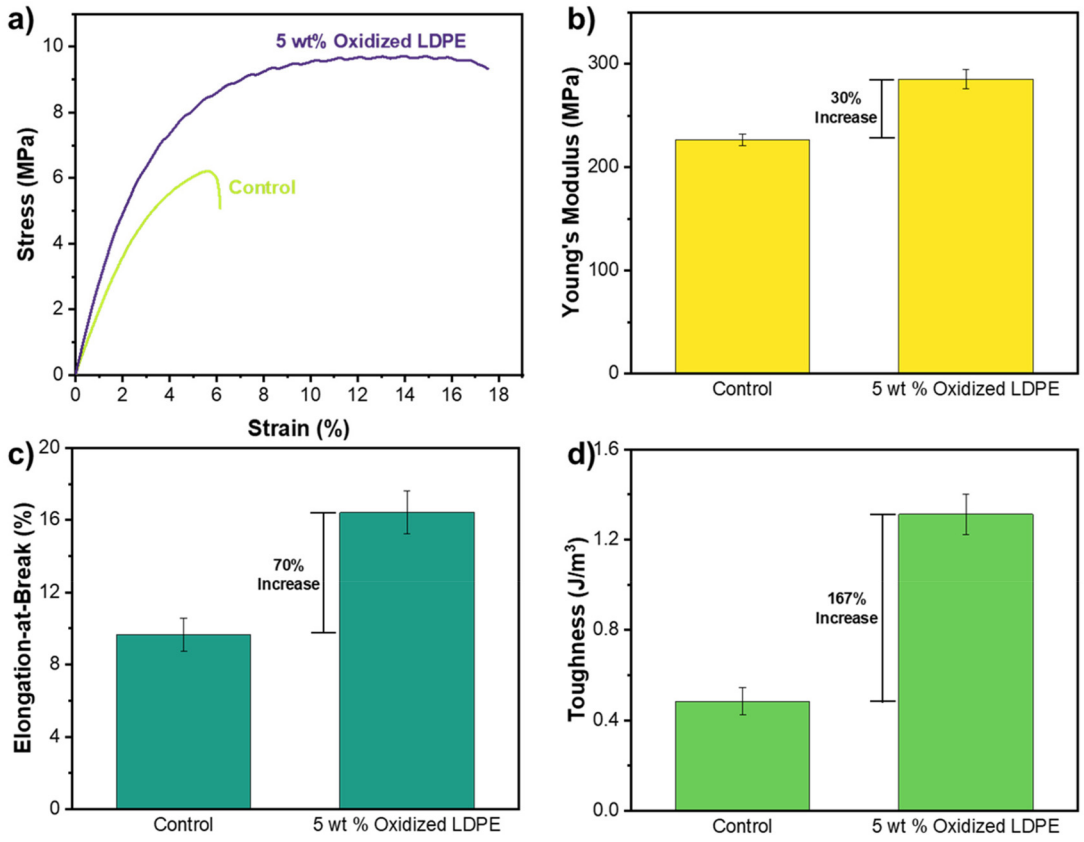

Fig. 7 (a) Example stress–strain curve, (b) Young's modulus, (c) elongation-at-break, and (d) toughness from tensile tests (10% per min) of control and plasma-oxidized blends at 5 wt%. The polymer blend is 70% LDPE (76 kg mol^{-1}) and 30% PLA with the addition of 5 wt% neat LDPE (40 kg mol^{-1}) acting as the control or plasma-oxidized LDPE (3.5% oxygen incorporation, 40 kg mol^{-1}) acting as compatibilizer. Plasma operating conditions for plasma-oxidized LDPE: treatment time: 2 h, O_2 feed molar percent: 2%, stir rate: 0 rpm, temperature: 150 °C, and LDPE to C_{28} ratio of 1 : 1. Errors represent the standard error across 6 replicates per sample type (n = 6).

All PLA/LDPE blends containing plasma-oxidized LDPE as a compatibilizer displayed improved tensile properties compared to controls with non-oxidized LDPE (Fig. 7a–d). The neat PLA displayed brittle behavior characterized by a Young's modulus of 982.4 MPa, an elongation-at-break of 3.2%, and a toughness of 0.55 J m^{-3} owing to its T_g (~53 °C) (Fig. S21 and Tables S3, S4). In contrast, the neat LDPE exhibited ductile behavior characterized by a Young's modulus of 169.2 MPa, an elongation-at-break of 85.5%, and a toughness of 6.0 J m^{-3} (Fig. S21 and Table S4). The control blend (LDPE, PLA, and 5 wt% non-oxidized LDPE) had a Young's modulus of 226.7 MPa, an elongation-at-break of 9.7%, and a toughness of 0.5 J m^{-3}. The resulting low elongation-at-break (*vs.* the primary LDPE phase) indicates an immiscible polymer blend with poor interfacial stress transfer and/or propagation. Introducing 5 wt% oxidized LDPE as a compatibilizer increased both Young's modulus by 30% (from 226.7 MPa to 285.4 MPa) and the elongation-at-break (from 9.7% to 16.4%) relative to the non-oxidized LDPE-containing control blend (Fig. 7 and Table S4). However, it worth noting that the Young's modulus is primarily governed by blend composition and is less impacted by interfacial adhesion.[70–72] Though outside the scope of this current study, the Young's modulus of the PE may have increased during the oxidation process due to the balance between crosslinking and scission reactions. Chain scission processes can reduce crystallinity by lowering the molecular weight and disrupting regular packing (Fig. 3 and Table S3), while the formation of crosslinks (Table S2) and polar groups also can result in strengthening the amorphous regions. Together, these effects may have led to an increase in the Young's modulus of the compatibilized system *vs.* the system containing the non-oxidized PE. This enhancement in Young's modulus and elongation-at-break values increased the toughness of the blends, defined as the amount of energy the sample can absorb before rupturing and calculated by integrating the area under the stress–strain curve. A 167% toughness increase in the oxidized blend over the control blend was observed (1.3 *vs.* 0.5 J m^{-3}) (Fig. 7 and Table S4). Additionally, the plasma-compatibilized blends were compared to a blend compatibilized with LDPE grafted with maleic anhydride (LDPE-gMAH), demonstrating a higher Young's modulus (285 *vs*. 206 MPa) and ultimate tensile strength (9.7 *vs.* 7.6 MPa), but a lower elongation-at-break (16.4 *vs*. 26.4%) at identical loadings (5 wt%). We hypothesize that adding the oxidized-LDPE or LDPE-gMAH compatibilizer improves interfacial interactions and phase-phase adhesion (*vs.* the non-oxidized-LDPE containing control), facilitating stress transfer and improving mechanical properties. This hypothesis is supported by SEM imaging, which shows a decrease in the repulsion between the LDPE and PLA phase and/or the number of visible voids (Fig. 6). Other mechanical testing parameters, such as ultimate tensile strength and stress-at-break, also improved for oxidized blends (Fig. S22 and Table S4).

To support our claims regarding improved interfacial interactions upon the addition of oxidized-LDPE to the PLA/LDPE blends, the interfacial tension between the blend components was estimated according to Wu's method [Methods, eqn (S5) and (S6)].[73] The addition of the plasma oxidized-LDPE to the PLA/LDPE blend reduces the estimated interfacial tension between PLA and LDPE from 3.81 to 2.95 mJ m^{-2} (Table S5). This reduction in the interfacial tension is attributed to an increase in the polar component (γ^p) and a decrease in the dispersive component (γ^d) of the interfacial tension of the base LDPE (from 6.0 to 19.2, and 21.9 to 8.5 mN m^{-2}, respectively) upon oxidized-LDPE incorporation (Table S6). Since the final blends included unfunctionalized or functionalized LDPE (~40 kg mol^{-1}), the improvement in mechanical properties was attributed directly to the oxygen groups along the polymer backbone of the plasma-treated material and the resulting reduced interfacial tension when blended with PLA.

Conclusions

This work demonstrated the plasma-induced, controlled oxidative functionalization of bulk PEW and PE of varying molecular weight by incorporating primarily hydroxyl and carbonyl (ketone and aldehyde) groups across the polymer backbone. The melting point, crystallinity, and molecular weight of the waxes decreased at elevated degrees of oxidation. In contrast, their thermal stability slightly increased, indicating an interplay between chain oxidation, scission, and cross-linking reactions. Compared to commercial oxidized waxes synthesized at high temperatures and pressures, plasma-oxidized waxes achieve similar acid numbers and oxidation percentages while featuring an increased diversity of functional groups. Direct extension to higher molecular weight polymers, such as LDPE of 40 and 76 kg mol^{-1}, is challenging due to the high bulk polymer melt viscosity. Controllable plasma oxidation occurs upon adding a long hydrocarbon (*e.g.*, *n*-octacosane) as a viscosity modifier to the LDPE melt, which can be easily removed by simple extraction methods. This viscosity modification provides a general strategy to achieve bulk functionalization of plastic waste, allowing waste upcycling and circularity across a broad range of polymer resin codes. Additionally, the long hydrocarbons can be produced by mild hydrogenolysis, and their oxidized products can be leveraged for several product markets. The plasma-oxidized LDPE can act as a compatibilizer for various phase-separating polymers such as LDPE and PLA polymer blends, considered here as a demonstration case. The incorporation of 5 wt% plasma-oxidized LDPE led to enhanced interfacial adhesion of the PLA/LDPE blend, as evidenced by SEM imaging and improved mechanical properties (70% increase in elongation-at-break values and 167% increase in toughness *vs*. the control blend). We anticipate that this compatibilization strategy could be extended to other immiscible systems representative of waste streams, such as poly(ethylene terephthalate)/polyolefin blends, by enhancing the polarity of the non-polar phase. Moreover, plasma modification enhances the polarity of LDPE (3.2-fold increase in γ^p), rendering it potentially suitable as a binding interlayer between polar and non-polar plastics for adhesion purposes.

In terms of catalyst-free oxidation, the main strategies typically include traditional thermal oxidation, biological/enzymatic oxidation, photochemical oxidation, and NTAP oxidation. Although traditional thermal oxidation has high scaling potential, it lacks selectivity due to overoxidation and requires significant energy input to activate C–H bonds.[74,75] Biological/enzymatic oxidation has shown success at low energy costs; however, it is difficult to scale and suffers from slow reaction rates.[76,77] Photochemical oxidation can also operate at low energy costs, but it is challenging to scale and is limited by slow reaction rates due to UV penetration constraints, making it primarily a surface oxidation technique.[78] Similarly, due to penetration constraints, conventional NTAP methods focus purely on surface oxidation techniques and usually require expensive vacuum systems, which are difficult to scale. The proposed NTAP oxidation method operates under atmospheric conditions and is capable of bulk polymer oxidation with high selectivity, overcoming a significant barrier. Additionally, due to the relatively simple configuration, this plasma process offers a decentralized approach to upcycling plastics waste, and implementation into plastics recycling plants could be potentially easier compared to other technologies.[79–81] A numbering-up strategy is well-suited for these smaller configurations, such as an array of pins impinging on a liquid surface or employing multiple plasma reactors in parallel, to increase production.[81] Optimizing the reactor geometry to increase the plasma–liquid interface, such as bubbling or use of microfluidics, can decrease the residence time and increase the production rate of oxidized LDPE.[39,80] However, this approach requires significant addition of viscosity modifiers to achieve efficient bulk oxidation, which necessitates downstream separations and raises potential scaling concerns. These challenges can be partially mitigated by using viscosity modifiers derived from more renewable sources (*e.g.*, PEWs) or by developing processes that do not require purified oxidized LDPE and can benefit from smaller hydrocarbon incorporation. Therefore, while further research and optimization are needed to scale up plasma processes as viable alternatives to conventional methods, this work opens a new avenue for utilizing plasma in chemical manufacturing, particularly for the upcycling of plastics waste. Overall, this work showcases a promising green, catalyst-free process for valorizing plastics waste that could be trialed for a broad range of plastics and associated blends and several hard-to-manufacture products.

Materials and methods

Chemicals

Oxygen (99.997%) and helium (99.999%) gases were purchased from KeenGas. Hexanes, *n*-octacosane (99%), *n*-hexadecane (99%), 1-hexandecanol (99%), 3-hexadecanone (98%), LDPE (weight-average molecular weight $\{M_w\}$ ~76 kg mol^{-1}), methylene chloride (>99.8%), tetrahydrofuran (>99.9%), dicumyl peroxide (DCP), maleic anhydride (MAH), and ethylene glycol (>99%) were purchased from Sigma-Aldrich. 1,1,2,2-tetrachloroethane-d_2 (>99%), 1,2,4-trichlorobenzene, and butylated hydroxytoluene were obtained from Fisher Scientific. LDPE (M_w ~40 kg mol^{-1}) was obtained from SciPoly. 4043D poly (lactic acid) (PLA) was obtained from Filabot. E 06 K PE wax, EO 75 K oxidized PE wax (5–9 acid number), and EO 78 K oxidized PE wax (20–24 acid number) were obtained by Deurex.

Plasma reactor and diagnostics

The plasma reactor design was detailed in our previous work.[40] Briefly, plasma oxidation of PE occurred in a pin-to-plate reactor configuration. PE pellets (~250 mg) were placed at the bottom of a glass reactor (17 mm diameter) heated using an external hotplate. A micro stir bar was added at the bottom of the glass reactor to induce convection in the polymer melt. To maintain a controlled gas atmosphere within the reactor, helium and oxygen gas mixtures were introduced (500 sccm) *via* mass flow controllers (Brooks GF 40 series). A high-voltage, stainless-steel pin was positioned above the melt surface, while a grounded, stainless-steel plate was placed at the exterior bottom of the glass vessel. The gap between the pin and plate was 7 mm, with the PE melt and glass vessel serving as dielectrics. Non-thermal, atmospheric-pressure plasma was generated using a direct current (DC) pulsed, high-voltage (HV) power supply (HVPPS1160 – High Voltage Laboratory, University of Patras). The peak-to-peak voltage, frequency, and duty cycle were kept constant at 9 kV, 5 kHz, and 1%, respectively, leading to a calculated dissipated power of ~1.9 W.

The voltage and current signals were recorded using a high-voltage probe (Tektronix P6015) and a current monitor (Pearson 6585). Both signals were acquired in real time using a Tektronix MDO32 wideband oscilloscope. A characteristic oscillogram is shown in Fig. S1. The average dissipated power (*i.e.*, the power consumed by the plasma discharge) was calculated using the following equation:

$$P = \frac{1}{T_p}\int_0^{T_p} v(t)i(t)\mathrm{d}t \quad (1)$$

in which T_p corresponds to the period of each wave, and $v(t)$ and $i(t)$ are the time-dependent voltage and current, respectively.

Optical emission spectroscopy (OES) measurements were performed using an AvaSpec-ULS4096CL-EVO spectrometer (Avantes). An optical fiber (400 μm) was used to collect the light emission from the plasma and the wideband emission spectrum in the region 300–900 nm was recorded and analyzed with the Avasoft software. A characteristic emission spectrum of the He/O_2 discharge is shown in Fig. S2.

Viscosity characterization

The viscosity of the starting waxes and polymers was determined using rheological tests on an ARES G2 rheometer (TA Instruments) equipped with either 25 mm stainless steel or 50 mm titanium parallel plates under N_2 flow. PE waxes were

loaded onto preheated 50 mm plates (110, 140, and 170 °C) and trimmed before testing at a gap of 0.5 mm. Prior to testing, a 60 s, 1 s^{-1} pre-shear was performed to remove any stresses arising during loading. Flow sweeps were performed from 50–1000 s^{-1} with a maximum equilibration time of 3 minutes. LDPE polymer samples were loaded onto preheated 25 mm plates (150 or 180 °C) and trimmed before testing at a gap of 0.5 mm. Prior to testing, a 60 s, 1 s^{-1} pre-shear was performed to remove any stresses arising during loading. Flow sweeps were performed from 0.1–100 s^{-1} (150 °C) and 10–100 s^{-1} (180 °C) with a maximum equilibration time of 3 min.

Product analysis

The resulting re-solidified product was analyzed using spectroscopic, thermal, and chromatogaphic characterizations to determine the resulting oxygen content and identify any changes to the properties of the polymer. To measure oxidation of the polymer, variable-temperature nuclear magnetic resonance (NMR) spectroscopy, Fourier-transform infrared (FTIR) spectroscopy, mirage-FTIR (mIRage), and X-ray photoelectron spectroscopy (XPS) were employed. For polymer property analysis, differential scanning calorimetry (DSC), thermogravimetric analysis (TGA), and high-temperature gel permeation chromatography (HT-GPC) were conducted.

Polymer oxidation

Surface analysis of the re-solidified product was conducted using FTIR, mIRage, and XPS. FTIR spectroscopy was performed on a Nicolet iS50 coupled with a golden gate diamond attenuated total reflectance module (ATR) and an MCTB detector at 4.0 cm^{-1} resolution using an average of 32 scans. MIRage sub-micron IR spectroscopy (Photothermal Spectroscopy Corp) was conducted on the cross-section of the molten product analyzing the IR range from 800–1920 cm^{-1}. XPS was performed using a Thermo Fisher K-Alpha instrument equipped with an Al (K) X-ray. Spectra were obtained with pass energies of 20, 10, and 20 eV for the survey, C 1s, and O 1s spectra, respectively, at 100 ms dwell time.

Bulk oxidation of the polymer chain was quantified using quantitative proton (^{1}H) NMR analysis[13] (AVIII 400 MHz spectrometer equipped with a Bruker BBO Probe and a BBI Probe). Prior to NMR, the polymer solid was dissolved in 1,1,2,2-tetrachloroethane-d_2 (TCE-d_2). NMR spectroscopy was conducted at 115 °C.

Untreated control ^{1}H NMR: (400 MHz, TCE-d_2) δ 0.9–1 (CH_3–*CH_2*–) 1.3–1.5 (–CH_2–).

Oxidized polymer ^{1}H NMR: (400 MHz, TCE-d_2) δ 0.9–1 (CH_3–*CH_2*–), 1.3–1.5 (–CH_2–), 2.4 (*CHO*–CH_2–), 3.6 (OH–*CH_2*–), 3.8 (–*CH_2*–CH_2O–*CH_2*–), 5.5 (–*CH_2*–$(CH)_2$–*CH_2*–), 9.8 (s, CHO–*CH_2*–).

The oxygen mol% corresponding to aldehyde, ketone, and primary and secondary alcohol incorporation along the backbone was determined quantitatively from the NMR spectra. The relative integrals between backbone CH_2 protons and proton peaks arising from, or adjacent to, oxygen-containing functional groups were calculated and converted to O_2 mol%. Full spectra, assignments, and example calculations are presented in Fig. S3.

Polymer crosslinking

The degree of polymer crosslinking was estimated by determining the gel fraction of samples *via* Soxhlet extraction in xylenes in a similar fashion to ASTM 2765-16. Polymer samples (~0.4 g) were loaded into washed cellulose thimbles and placed within the Soxhlet apparatus. The flask was filled with 200 mL of xylenes and heated (~160 °C) to achieve ~10 min extraction cycles. After the first extraction cycle, the process was continued for 24 h. The resulting insoluble fraction was vacuum dried at 70 °C for 24 h and weighed.

Thermal analysis

DSC was conducted on a Discovery DSC (TA Instruments). Samples (~5 mg) were sealed in an aluminum T_{zero} pan with lids. Samples were equilibrated to 30 °C, ramped to 200 °C at 10 °C min^{-1}, cooled at 10 °C min^{-1} to −50 °C, before being ramped to 200 °C, under N_2 atmosphere. Analyses were performed on second heating traces on TRIOS software (TA Instruments) unless specified otherwise. Crystallinities were calculated according to eqn (2). ΔH_m and ΔH_c are the melting and cold crystallization (if present) enthalpies of the sample, respectively, and ΔH_m° is the melting enthalpy (293 J g^{-1}) of the perfect PE crystal.[46]

$$\%\ \text{crystallinity} = \frac{\Delta H_m - \Delta H_c}{\Delta H_m^\circ} \times 100 \quad (2)$$

TGA was performed on a Discovery TGA (TA Instruments). Samples were ramped from 40 °C to 600 °C at 10 °C min^{-1} under N_2 atmosphere. Analyses were performed using the TRIOS software (TA Instruments) unless specified otherwise.

HT-GPC

Molecular weight characterization of oxidized and non-oxidized PE products was conducted using a HLC-8312GPC/HT HT-GPC (TOSOH Bioscience) in 1,2,4-trichlorobenzene. Samples were dissolved in the mobile phase (1,2,4-trichlorobenzene with 500 ppm BHT) at ~2 mg mL^{-1} concentration and dissolved under stirring for 2 h at 140 °C. 300 μL injections of sample solutions were eluted at 0.8 mL min^{-1} at 140 °C through two TSKgel GMHHR-H(20)HT columns in series, with refractive index (RI) and differential viscometer detectors. Molecular weight calculations were calibrated using 12 narrow polystyrene standards (6×10^2–2×10^6 g mol^{-1}) and corrected according to the Mark–Houwink relationships for PE (according to prior work[82]).

Solvent extraction & quantification

n-octacosane was added to LDPE to reduce the viscosity. After oxidation, 7 mL of hexanes was added to the solid melt and sonicated for 15 min to extract the *n*-octacosane (C_{28}) and corresponding oxygenates from the solidified LDPE melt. The solids were filtered and dried in an oven at 75 °C overnight.

This process was repeated twice to ensure complete extraction of the lower molecular weight compounds from the LDPE. For quantification of extracted *n*-octacosane and corresponding oxygenates, the dissolved products were analyzed using a gas chromatography–flame ionization detector (GC-FID) (Agilent 7890B) with an Agilent J&W HP-INNOWax column (30 m, 0.25 mm, 0.25 μm) and GC-MS (Shimadzu GCMS-QP2010) with an Agilent J&W HP-INNOWax column (30 m, 0.25 mm, 0.25 μm). Calibration curves were constructed using external standards of *n*-hexadecane, 1-hexadecanol, and 3-hexadecanone and adjusted to the response factor of *n*-octacosane. The conversion of *n*-alkane was calculated as follows.

$$n\text{-Alkane conversion}\,(\%) = \frac{nC_i - nC_f}{nC_i} \times 100\% \quad (3)$$

where nC_i corresponds to the initial moles of carbon in the reactant, and nC_f corresponds to the unreacted moles of carbon. The product yield was determined by eqn (4).

$$\text{Product yield}\,(\%) = \frac{nC_{product}}{nC_i} \times 100\% \quad (4)$$

where $nC_{product}$ refers to the moles of carbon in the oxygenated products and nC_i is the initial moles of carbon in the *n*-alkane.

For gas-phase analysis, gas-sampling bags were used to collect the reactor's output at sequential times throughout the plasma experiments and analyzed using a Micro GC (Agilent 990), which allows the quantification of CH_4, C_2H_6, C_2H_4, CO_2, O_2, *etc*. Gaseous components, such as CO_2 and O_2, were quantified using external standard calibrations. To assess the possible formation of lighter gaseous species and evaporation, the outlet gas was bubbled through an acetone solvent trap in an ice bath and analyzed in the GC.

Generation of polymer blends, characterization, and testing

Polymer blends were produced using a MiniLab III microcompounder (Thermo Scientific) at 200 °C under an N_2 atmosphere with a screw speed of 100 rpm. Samples were compounded for 3 min under "cycle" mode before extruding into filaments and left to cool in air. 70 wt% LDPE (M_w ~76 kg mol^{-1}) and 30 wt% PLA were compounded with 5 wt% of neat LDPE (M_w ~40 kg mol^{-1}), plasma-oxidized LDPE (M_w ~40 kg mol^{-1}) to produce controls and samples. Additional samples for interfacial testing were produced by blending 5 wt% plasma-oxidized LDPE (M_w ~40 kg mol^{-1}) with LDPE (M_w ~76 kg mol^{-1}). Supplemental LDPE-gMAH samples were generated by blending 40 kg mol^{-1} LDPE with 0.1 wt% DCP (initiator) and 1.5 wt% MAH using the conditions described above (confirmed *via* FTIR Fig. S23). The LDPE-gMAH was then compounded with 70 wt% LDPE (M_w ~ 76 kg mol^{-1}) and 30 wt% PLA at identical conditions.

Thermal properties of the LDPE/PLA polymer blends with and without compatibilizer were analyzed using DSC and TGA as previously described. Crystallinities were calculated according to eqn (5). ΔH_m and ΔH_c are the melting and cold crystallization (if present) enthalpies of the sample, respectively, ΔH_m° is the melting enthalpy (293 J g^{-1}) of either a perfect PE crystal[46] or (93 J g^{-1}) PLA crystal,[83] and w_i is the weight fraction of the polymer in the blend.

$$\%\ \text{crystallinity} = \frac{\Delta H_m - \Delta H_c}{w_i \times \Delta H_m^\circ} \times 100 \quad (5)$$

To visualize LDPE/PLA phase behavior, scanning electron microscopy (SEM) was conducted on the polymer blends using a JEOL JSM 7400F-SEM. Samples were immersed in liquid N_2, fractured, and sputter-coated with a thin layer of gold-palladium alloy for 60 s before imaging.

Tensile testing was conducted on LDPE/PLA polymer blends with and without compatibilizer using a Zwick/Roell Z 0.5 (500 N zwicki-Line) tensile tester with a 200 N load cell, a clamp force of 200 N, and tested at a constant strain rate of 10% per min. Prior to tensile testing, all LDPE/PLA polymer blends with and without compatibilizer were pressed into films using a hot press with pre-heated plates at 200 °C for 30 s at ~ 500 psi. Samples were then cut from molded films using a specialized cutter to produce dumbbell samples with dimensions of ~9.5 mm × ~2.5 mm × ~0.1 mm (Fig. S4). The Young's modulus was calculated from the linear region of the stress–strain curves.

Contact angle analysis was performed using a VCA Optima (AST Products Inc.) video contact angle system. Prior to testing, PLA, LDPE, and LDPE + 5 wt% O-LDPE were pressed into films using a hot press with pre-heated plates at 200 °C for 30 s at ~500 psi. The contact angle between the polymer sample and water and ethylene glycol was analyzed *via* the ImageJ contact angle plug-in tool. The surface tension between PLA/LDPE and PLA/LDPE + O-LDPE was estimated according to Wu's method.[73,84,85] Briefly, by measuring the contact angle between a material and two liquids with known dispersive (γ^d) and polar (γ^p) components of surface tension ($\gamma = \gamma^d + \gamma^p$), γ^d and γ^p of the material can be estimated using:

$$(1 + \cos\theta)\gamma_L = \frac{4\gamma_S^d\gamma_L^d}{\gamma_S^d + \gamma_L^d} + \frac{4\gamma_S^p\gamma_L^p}{(\gamma_S^p + \gamma_L^p)} \quad (6)$$

where γ_L is the surface tension of the liquid, θ is the measured contact angle between the liquid and the solid, γ_S^d and γ_L^d are the dispersive components of the interfacial tension of the solid and the liquid, respectively, and γ_S^p and γ_L^p are the polar components of the interfacial tension of the solid and liquid respectively. Since γ_L^d and γ_L^p are known values (water: 21.8 and 51.0 mJ m^{-2}, respectively; ethylene glycol: 29.0 and 21.8 mJ m^{-2}, respectively),[86] the interfacial tension between the two polymers (1 and 2) can be calculated *via*:

$$\gamma_{1,2} = \gamma_1 + \gamma_2 + \frac{4{\gamma_1}^d{\gamma_2}^d}{{\gamma_1}^d + {\gamma_2}^2} + \frac{4{\gamma_1}^p{\gamma_2}^p}{({\gamma_1}^p + {\gamma_2}^p)} \quad (7)$$

where γ^d and γ^p are the dispersive and polar components of the surface tension of the two polymers (subscripts 1 and 2), and $\gamma_{1,2}$ is the interfacial tension between two polymers (1 and 2).

Author contributions

Conceptualization: DKN, ZOGS, LTJK, DGV. Methodology: DKN, ZOGS, LTJK, DGV. Investigation: DKN, ZOGS. Visualization: DKN, ZOGS. Funding acquisition: LTJK, DGV. Project administration: LTJK, DGV. Supervision: LTJK, DGV. Writing – original draft: DKN, ZOGS. Writing – review & editing: DKN, ZOGS, LTJK, DGV.

Conflicts of interest

The authors have a patent application for this process.

Data availability

The data supporting this article have been included as part of the Supplementary Information: electrical waveforms; optical emission spectroscopy spectrum; NMR SI; images of tensile testing molds; XPS survey spectra; mIRage of oxidized PEW cross-section; gravimetric and CO_2 analysis for PEW; proposed reaction network; rheological characterization of PEWs; sample integrated DSC curve; DSC values for PEW; first derivative TGA weight loss graphs for PEW; DSC, TGA, GPC comparison to commercial waxes; oxidation of neat 40 kg mol^{-1} LDPE; rheological characterization of neat 40 kg mol^{-1} LDPE; gravimetric analysis for neat 40 kg mol^{-1} LDPE; ^1H NMR spectra for plasma-oxidized 40 kg mol^{-1} LDPE; conversion and product yield of plasma-oxidized C_{28}; plasma oxidation of 76 kg mol^{-1} LDPE; DSC, TGA, and GPC of plasma-oxidized 40 kg mol^{-1} LDPE; DSC values for 40 kg mol^{-1} LDPE; DSC and TGA of polymer blends; DSC values for polymer blends; stress–strain curves of neat LDPE and PLA; mechanical properties of neat polymers and blends; interfacial tension estimates of compatibilized blends; confirming grafting of MAH on LDPE. See DOI: **https://doi.org/10.1039/d5gc02799c**.

Acknowledgements

The plasma work of D. K. N. was supported by the U.S. National Science Foundation under award number 2134471. The polymer-based work of Z. O. G. S. was supported as part of the Center for Plastics Innovation, an Energy Frontier Research Center funded by the US Dept. of Energy, Office of Science, Office of Basic Energy Sciences under award number DE-SC0021166. We thank the Advanced Materials Characterization lab at the University of Delaware for FTIR instrument time. XPS analysis was performed with the instrument sponsored by the National Science Foundation under grant No. CHE-1428149. The authors acknowledge the use of NMR facilities and instrumentation (AVIII 400) supported by the National Institutes of Health under Award Number S10RR026962-01.

References

1 N. Rustagi, S. K. Pradhan and R. Singh, Public health impact of plastics: An overview, *Indian J. Occup. Environ. Med.*, 2011, **15**(3), 100–103, DOI: **10.4103/0019-5278.93198**, From NLM.
2 A. Rahimi and J. M. García, Chemical recycling of waste plastics for new materials production, *Nat. Rev. Chem.*, 2017, **1**(6), 0046, DOI: **10.1038/s41570-017-0046**.
3 R. Geyer, Production, use, and fate of synthetic polymers, in *Plastic Waste and Recycling*, ed. T. M. Letcher, Academic Press, 2020, ch. 2, pp. 13–32.
4 T. F. Astrup, D. Tonini, R. Turconi and A. Boldrin, Life cycle assessment of thermal Waste-to-Energy technologies: Review and recommendations, *Waste Manage.*, 2015, **37**, 104–115, DOI: **10.1016/j.wasman.2014.06.011**.
5 A. Vlasopoulos, J. Malinauskaite, A. Żabnieńska-Góra and H. Jouhara, Life cycle assessment of plastic waste and energy recovery, *Energy*, 2023, **277**, 127576, DOI: **10.1016/j.energy.2023.127576**.
6 D. Baca, R. Monroy, M. Castillo, A. Elkhazraji, A. Farooq and R. Ahmad, Dioxins and plastic waste: A scientometric analysis and systematic literature review of the detection methods, *Environ. Adv.*, 2023, **13**, 100439, DOI: **10.1016/j.envadv.2023.100439**.
7 G. G. N. Thushari and J. D. M. Senevirathna, Plastic pollution in the marine environment, *Heliyon*, 2020, **6**(8), e04709, DOI: **10.1016/j.heliyon.2020.e04709**.
8 R. Lehner, C. Weder, A. Petri-Fink and B. Rothen-Rutishauser, Emergence of Nanoplastic in the Environment and Possible Impact on Human Health, *Environ. Sci. Technol.*, 2019, **53**(4), 1748–1765, DOI: **10.1021/acs.est.8b05512**.
9 R. Balu, N. K. Dutta and N. Roy Choudhury, Plastic, Waste Upcycling: A Sustainable Solution for Waste Management, Product Development, and Circular Economy, *Polymers*, 2022, **14**(22), 4788.
10 Z. Jianyu, Y. Yongjie, G. Jinsheng and X. Jianhang, Development of oxidized polyethylene waxes, *Pet. Sci. Technol.*, 2000, **18**(9–10), 1077–1088, DOI: **10.1080/10916460008949892**.
11 A. J. Zervoudakis, C. S. Sample, X. Peng, D. Lake, M. A. Hillmyer and C. J. Ellison, Dihydroxy Polyethylene Additives for Compatibilization and Mechanical Recycling of Polyethylene Terephthalate/Polyethylene Mixed Plastic Waste, *ACS Macro Lett.*, 2022, **11**(12), 1396–1402, DOI: **10.1021/acsmacrolett.2c00601**.
12 M. T. Savoji, D. Zhao, R. J. Muisener, K. Schimossek, K. Schoeller, T. P. Lodge and M. A. Hillmyer, Poly(alkyl methacrylate)-Grafted Polyolefins as Viscosity Modifiers for Engine Oil: A New Mechanism for Improved Performance, *Ind. Eng. Chem. Res.*, 2018, **57**(6), 1840–1850, DOI: **10.1021/acs.iecr.7b04634**.
13 L. Chen, K. G. Malollari, A. Uliana, D. Sanchez, P. B. Messersmith and J. F. Hartwig, Selective, Catalytic Oxidations of C–H Bonds in Polyethylenes Produce

Functional Materials with Enhanced Adhesion, *Chem*, 2021, **7**(1), 137–145, DOI: **10.1016/j.chempr.2020.11.020**.

14 J. Maris, S. Bourdon, J.-M. Brossard, L. Cauret, L. Fontaine and V. Montembault, Mechanical recycling: Compatibilization of mixed thermoplastic wastes, *Polym. Degrad. Stab.*, 2018, **147**, 245–266, DOI: **10.1016/j.polymdegradstab.2017.11.001**.

15 C. M. Plummer, L. Li and Y. Chen, The post-modification of polyolefins with emerging synthetic methods, *Polym. Chem.*, 2020, **11**(43), 6862–6872, DOI: **10.1039/D0PY01279C**.

16 L. S. Boffa and B. M. Novak, Copolymerization of Polar Monomers with Olefins Using Transition-Metal Complexes, *Chem. Rev.*, 2000, **100**(4), 1479–1494, DOI: **10.1021/cr990251u**.

17 N. K. Boaen and M. A. Hillmyer, Post-polymerization functionalization of polyolefins, *Chem. Soc. Rev.*, 2005, **34**(3), 267–275, DOI: **10.1039/B311405H**.

18 W.-j. Tao, R. Nakano, S. Ito and K. Nozaki, Copolymerization of Ethylene and Polar Monomers by Using Ni/IzQO Catalysts, *Angew. Chem., Int. Ed.*, 2016, **55**(8), 2835–2839, DOI: **10.1002/anie.201510077**.

19 M. Baur, F. Lin, T. O. Morgen, L. Odenwald and S. Mecking, Polyethylene materials with in-chain ketones from nonalternating catalytic copolymerization, *Science*, 2021, **374**(6567), 604–607, DOI: **10.1126/science.abi8183**.

20 M. A. Gauthier, M. I. Gibson and H.-A. Klok, Synthesis of Functional Polymers by Post-Polymerization Modification, *Angew. Chem., Int. Ed.*, 2009, **48**(1), 48–58, DOI: **10.1002/anie.200801951**, (acccessed 2024/10/23).

21 R. Lemmens, J. Vercammen, L. Van Belleghem and D. De Vos, Upcycling polyethylene into closed-loop recyclable polymers through titanosilicate catalyzed C-H oxidation and in-chain heteroatom insertion, *Nat. Commun.*, 2024, **15**(1), 9188, DOI: **10.1038/s41467-024-53506-9**.

22 J. X. Shi, N. R. Ciccia, S. Pal, D. D. Kim, J. N. Brunn, C. Lizandara-Pueyo, M. Ernst, A. M. Haydl, P. B. Messersmith, B. A. Helms, *et al.*, Chemical Modification of Oxidized Polyethylene Enables Access to Functional Polyethylenes with Greater Reuse, *J. Am. Chem. Soc.*, 2023, **145**(39), 21527–21537, DOI: **10.1021/jacs.3c07186**.

23 U. Yolsal, T. J. Neal, J. A. Richards, J. R. Royer and J. A. Garden, A versatile modification strategy to enhance polyethylene properties through solution-state peroxide modifications, *Polym. Chem.*, 2024, **15**(14), 1399–1412, DOI: **10.1039/d3py01399e**.

24 R. J. Kelly, Review of Safety Guidelines for Peroxidizable Organic Chemicals, *Chem. Health Saf.*, 1996, **3**(5), 28–36, DOI: **10.1021/acs.chas.8b03515**.

25 J. B. Williamson, S. E. Lewis, R. R. Johnson III, I. M. Manning and F. A. Leibfarth, C–H Functionalization of Commodity Polymers, *Angew. Chem., Int. Ed.*, 2019, **58**(26), 8654–8668, DOI: **10.1002/anie.201810970**.

26 E. Passaglia, S. Coiai, F. Cicogna and F. Ciardelli, Some recent advances in polyolefin functionalization, *Polym. Int.*, 2014, **63**(1), 12–21, DOI: **10.1002/pi.4598**.

27 L. Bárdos and H. Baránková, Plasma processes at atmospheric and low pressures, *Vacuum*, 2008, **83**(3), 522–527, DOI: **10.1016/j.vacuum.2008.04.063**.

28 L. Bárdos and H. Baránková, Cold atmospheric plasma: Sources, processes, and applications, *Thin Solid Films*, 2010, **518**(23), 6705–6713, DOI: **10.1016/j.tsf.2010.07.044**.

29 A. Bogaerts, E. Neyts, R. Gijbels and J. van der Mullen, Gas discharge plasmas and their applications, *Spectrochim. Acta, Part B*, 2002, **57**(4), 609–658, DOI: **10.1016/S0584-8547(01)00406-2**.

30 R. J. Wandell and B. R. Locke, Hydrocarbon Processing by Plasma, in *Springer Handbook of Petroleum Technology*, Springer International Publishing, 2017, pp. 1163–1182.

31 P. J. Bruggeman, F. Iza and R. Brandenburg, Foundations of atmospheric pressure non- equilibrium plasmas, *Plasma Sources Sci. Technol.*, 2017, **26**, 123002, DOI: **10.1088/1361-6595/aa97af**, (acccessed 2023-04-13T20:06:35).

32 P. Bruggeman and C. Leys, Non-thermal plasmas in and in contact with liquids, *J. Phys. D: Appl. Phys.*, 2009, **42**, 053001, DOI: **10.1088/0022-3727/42/5/053001**, (acccessed 2023-04-13T20:02:41).

33 Y. W. Hsiao, D. K. Nguyen, K. Yu, W. Zheng, P. Dimitrakellis and D. G. Vlachos, Enhanced Catalytic Hydrodeoxygenation of Activated Carbon-Supported Metal Catalysts via Rapid Plasma Surface Functionalization, *ACS Appl. Mater. Interfaces*, 2023, **15**(22), 26737–26745, DOI: **10.1021/acsami.3c03447**.

34 A. Popelka, P. N. Khanam and M. A. AlMaadeed, Surface modification of polyethylene/graphene composite using corona discharge, *J. Phys. D:Appl. Phys.*, 2018, **51**(10), 105302, DOI: **10.1088/1361-6463/aaa9d6**.

35 J.-P. Booth, M. Mozetič, A. Nikiforov and C. Oehr, Foundations of plasma surface functionalization of polymers for industrial and biological applications, *Plasma Sources Sci. Technol.*, 2022, **31**(10), 103001, DOI: **10.1088/1361-6595/ac70f9**.

36 J. Carneiro de Oliveira, A. Airoudj, P. Kunemann, F. Bally-Le Gall and V. Roucoules, Mechanical properties of plasma polymer films: a review, *SN Appl. Sci.*, 2021, **3**(6), 656, DOI: **10.1007/s42452-021-04655-9**.

37 V. Švorčík, K. Kolářová, P. Slepička, A. Macková, M. Novotná and V. Hnatowicz, Modification of surface properties of high and low density polyethylene by Ar plasma discharge, *Polym. Degrad. Stab.*, 2006, **91**(6), 1219–1225, DOI: **10.1016/j.polymdegradstab.2005.09.007**.

38 M. Goldman, M. Lee, R. Gronsky and L. Pruitt, Oxidation of ultrahigh molecular weight polyethylene characterized by Fourier Transform Infrared Spectrometry, *J. Biomed. Mater. Res.*, 1997, **37**(1), 43–50, DOI: **10.1002/(SICI)1097-4636(199710)37:1<43::AID-JBM6>3.0.CO;2-J**.

39 D. K. Nguyen, F. Cameli, P. Dimitrakellis and D. G. Vlachos, Biphasic Plasma Microreactor for Oxyfunctionalization of Liquid Hydrocarbons, *Ind. Eng. Chem. Res.*, 2024, **63**(20), 9008–9017, DOI: **10.1021/acs.iecr.4c00605**.

40 D. K. Nguyen, P. Dimitrakellis, M. R. Talley, R. M. O'Dea, T. H. Epps III, M. P. Watson and D. G. Vlachos, Oxidative

Functionalization of Long-Chain Liquid Alkanes by Pulsed Plasma Discharges at Atmospheric Pressure, *ACS Sustainable Chem. Eng.*, 2022, **10**(48), 15749–15759, DOI: 10.1021/acssuschemeng.2c04269.

41 P. Patiño, M. Méndez, J. Pastrán, G. Gambús, J. Navea, O. Escobar and A. Castro, Oxidation of Cycloalkanes and Diesel Fuels by Means of Oxygen Low Pressure Plasmas, *Energy Fuels*, 2002, **16**(6), 1470–1475, DOI: 10.1021/ef020068v, (acccessed 2023-04-13T20:37:55).

42 G. Gambús, P. Patiño, B. Méndez, A. Sifontes, J. Navea, P. Martín and P. Taylor, Oxidation of Long Chain Hydrocarbons by Means of Low-Pressure Plasmas, *Energy Fuels*, 2001, **15**(4), 881–886, DOI: 10.1021/ef000271v, (acccessed 2023-04-13T20:37:25).

43 S. V. Kudryashov, G. S. Shchegoleva, E. E. Sirotkina and A. Y. Ryabov, Oxidation of hydrocarbons in a barrier discharge reactor, *High Energy Chem.*, 2000, **34**(2), 112–115, DOI: 10.1007/bf02761839, (acccessed 2023-04-13T20:38:21).

44 L. J. Gerenser, XPS studies of in situ plasma-modified polymer surfaces, *J. Adhes. Sci. Technol.*, 1993, **7**(10), 1019–1040, DOI: 10.1163/156856193X00556.

45 L.-K. Ju and C. S. Ho, The measurement of oxygen diffusion coefficients in polymeric solutions, *Chem. Eng. Sci.*, 1986, **41**(3), 579–589, DOI: 10.1016/0009-2509(86)87040-3.

46 Y. Kong and J. N. Hay, The measurement of the crystallinity of polymers by DSC, *Polymer*, 2002, **43**(14), 3873–3878, DOI: 10.1016/S0032-3861(02)00235-5.

47 A. Smedberg, T. Hjertberg and B. Gustafsson, Crosslinking reactions in an unsaturated low density polyethylene, *Polymer*, 1997, **38**(16), 4127–4138, DOI: 10.1016/S0032-3861(96)00994-9.

48 Y.-T. Shieh and T.-H. Tsai, Silane grafting reactions of low-density polyethylene, *J. Appl. Polym. Sci.*, 1998, **69**(2), 255–261, DOI: 10.1002/(SICI)1097-4628(19980711)69:2<255::AID-APP6>3.0.CO;2-M.

49 P. L. Durrill and R. G. Griskey, Diffusion and solution of gases into thermally softened or molten polymers: Part II. Relation of diffusivities and solubilities with temperature pressure and structural characteristics, *AIChE J.*, 1969, **15**(1), 106–110, DOI: 10.1002/aic.690150124.

50 A. K. O'Brien and C. N. Bowman, Impact of Oxygen on Photopolymerization Kinetics and Polymer Structure, *Macromolecules*, 2006, **39**(7), 2501–2506, DOI: 10.1021/ma051863l.

51 P. A. Kots, B. C. Vance and D. G. Vlachos, Polyolefin plastic waste hydroconversion to fuels, lubricants, and waxes: a comparative study, *React. Chem. Eng.*, 2022, **7**(1), 41–54, DOI: 10.1039/d1re00447f, (acccessed 2023-04-13T18:29:43).

52 R. R. J. Cerpentier, T. van Vliet, L. V. Pastukhov, M. van Drongelen, M. J. Boerakker, T. A. Tervoort and L. E. Govaert, Fatigue-Crack Propagation of High-Density Polyethylene Homopolymers: Influence of Molecular Weight Distribution and Temperature, *Macromolecules*, 2021, **54**(24), 11508–11521, DOI: 10.1021/acs.macromol.1c01945.

53 S. M. Kurtz, 1 – A Primer on UHMWPE, in *UHMWPE Biomaterials Handbook*, ed. S. M. Kurtz, William Andrew Publishing, 3rd edn, 2016, pp. 1–6.

54 Y. Sui, Z. Qiu, Y. Liu, J. Li, Y. Cui, P. Wei, C. Cong, X. Meng and Q. Zhou, Ultra-high molecular weight polyethylene (UHMWPE)/high-density polyethylene (HDPE) blends with outstanding mechanical properties, wear resistance, and processability, *J. Polym. Res.*, 2023, **30**(6), 222, DOI: 10.1007/s10965-023-03592-y.

55 A. Paajanen, J. Vaari and T. Verho, Crystallization of cross-linked polyethylene by molecular dynamics simulation, *Polymer*, 2019, **171**, 80–86, DOI: 10.1016/j.polymer.2019.03.040.

56 D. Vrsaljko, D. Macut and V. Kovačević, Potential role of nanofillers as compatibilizers in immiscible PLA/LDPE Blends, *J. Appl. Polym. Sci.*, 2015, **132**(6), 41414, DOI: 10.1002/app.41414.

57 C. M. Thurber, Y. Xu, J. C. Myers, T. P. Lodge and C. W. Macosko, Accelerating Reactive Compatibilization of PE/PLA Blends by an Interfacially Localized Catalyst, *ACS Macro Lett.*, 2015, **4**(1), 30–33, DOI: 10.1021/mz500770y.

58 V. Lovinčić Milovanović, I. Hajdinjak, I. Lovriša and D. Vrsaljko, The influence of the dispersed phase on the morphology, mechanical and thermal properties of PLA/PE-LD and PLA/PE-HD polymer blends and their nanocomposites with TiO_2 and $CaCO_3$, *Polym. Eng. Sci.*, 2019, **59**(7), 1395–1408, DOI: 10.1002/pen.25124.

59 L. Gu and C. W. Macosko, Evaluating PE/PLA interfacial tension using ternary immiscible polymer blends, *J. Appl. Polym. Sci.*, 2021, **138**(26), 50623, DOI: 10.1002/app.50623.

60 C. A. Gracia-Fernández, S. Gómez-Barreiro, J. López-Beceiro, S. Naya and R. Artiaga, New approach to the double melting peak of poly(l-lactic acid) observed by DSC, *J. Mater. Res.*, 2012, **27**(10), 1379–1382, DOI: 10.1557/jmr.2012.57.

61 T. Tábi, S. Hajba and J. G. Kovács, Effect of crystalline forms (α′ and α) of poly(lactic acid) on its mechanical, thermo-mechanical, heat deflection temperature and creep properties, *Eur. Polym. J.*, 2016, **82**, 232–243, DOI: 10.1016/j.eurpolymj.2016.07.024.

62 K. M. Van de Voorde, J. K. Pokorski and L. T. J. Korley, Exploring Morphological Effects on the Mechanics of Blended Poly(lactic acid)/Poly(ε-caprolactone) Extruded Fibers Fabricated Using Multilayer Coextrusion, *Macromolecules*, 2020, **53**(13), 5047–5055, DOI: 10.1021/acs.macromol.0c00289.

63 S. E. Fenni, J. Wang, N. Haddaoui, B. D. Favis, A. J. Müller and D. Cavallo, Crystallization and self-nucleation of PLA, PBS and PCL in their immiscible binary and ternary blends, *Thermochim. Acta*, 2019, **677**, 117–130, DOI: 10.1016/j.tca.2019.03.015.

64 J. G. Fatou and L. Mandelkern, The Effect of Molecular Weight on the Melting Temperature and Fusion of Polyethylene1, *J. Phys. Chem.*, 1965, **69**(2), 417–428, DOI: 10.1021/j100886a010.

65 S. A. Jabarin, K. Majdzadeh-Ardakani and E. A. Lofgren, Crystallization and Melting Behavior in Polymer Blends, in *Encyclopedia of Polymer Blends*, 2016, pp. 135–190.

66 S. Kobayashi and K. Müllen, *Encyclopedia of polymeric nanomaterials*, Springer Reference, 2015. DOI: 10.1007/978-3-642-29648-2.
67 N. Z. Tomić, Thermal studies of compatibilized polymer blends, in *Compatibilization of Polymer Blends*, ed. A. A. Ramachandran and S. Thomas, Elsevier, 2020, ch. 17, pp. 489–510.
68 D. R. Paul and J. W. Barlow, Polymer Blends, *J. Macromol. Sci., Part C*, 1980, **18**(1), 109–168, DOI: 10.1080/00222358008080917.
69 H. Ahmadi, P. M. H. van Heugten, A. Veber, L. Puskar, P. D. Anderson and R. Cardinaels, Toughening Immiscible Polymer Blends: The Role of Interface-Crystallization-Induced Compatibilization Explored Through Nanoscale Visualization, *ACS Appl. Mater. Interfaces*, 2024, **16**(43), 59174–59187, DOI: 10.1021/acsami.4c10829.
70 Z. H. Liu, P. Maréchal and R. Jérôme, Blends of poly(vinylidene fluoride) with polyamide 6: interfacial adhesion, morphology and mechanical properties, *Polymer*, 1998, **39**(10), 1779–1785, DOI: 10.1016/S0032-3861(97)00222-X.
71 J. Kolarik, Simultaneous prediction of the modulus and yield strength of binary polymer blends, *Polym. Eng. Sci.*, 1996, **36**(20), 2518–2524, DOI: 10.1002/pen.10650.
72 B. Pukánszky and F. Tüdõs, Miscibility and mechanical properties of polymer blends, *Makromol. Chem. Macromol. Symp.*, 1990, **38**(1), 221–231, DOI: 10.1002/masy.19900380118.
73 S. Wu, Calculation of interfacial tension in polymer systems, *J. Polym. Sci., Part C: Polym. Symp.*, 1971, **34**(1), 19–30, DOI: 10.1002/polc.5070340105.
74 D. M. Brown, A. Fish and T. M. Sugden, The extension to long-chain alkanes and to high temperatures of the hydroperoxide chain mechanism of autoxidation, *Proc. R. Soc. London, Ser. A*, 1969, **308**(1495), 547–568, DOI: 10.1098/rspa.1969.0025.
75 Z. Wang, M. Ehn, M. P. Rissanen, O. Garmash, L. Quéléver, L. Xing, M. Monge-Palacios, P. Rantala, N. M. Donahue, T. Berndt, *et al.*, Efficient alkane oxidation under combustion engine and atmospheric conditions, *Commun. Chem.*, 2021, **4**(1), 18, DOI: 10.1038/s42004-020-00445-3.
76 Y.-F. Liu, J. Chen, Z.-L. Liu, L.-B. Shou, D.-D. Lin, L. Zhou, S.-Z. Yang, J.-F. Liu, W. Li, J.-D. Gu, *et al.*, Anaerobic Degradation of Paraffins by Thermophilic Actinobacteria under Methanogenic Conditions, *Environ. Sci. Technol.*, 2020, **54**(17), 10610–10620, DOI: 10.1021/acs.est.0c02071.
77 F. Rojo, Degradation of alkanes by bacteria, *Environ. Microbiol.*, 2009, **11**(10), 2477–2490, DOI: 10.1111/j.1462-2920.2009.01948.x.
78 A. L. Andrady, P. W. Barnes, J. F. Bornman, T. Gouin, S. Madronich, C. C. White, R. G. Zepp and M. A. K. Jansen, Oxidation and fragmentation of plastics in a changing environment; from UV-radiation to biological degradation, *Sci. Total Environ.*, 2022, **851**, 158022, DOI: 10.1016/j.scitotenv.2022.158022.
79 E. Delikonstantis, F. Cameli, M. Scapinello, V. Rosa, K. M. Van Geem and G. D. Stefanidis, Low-carbon footprint chemical manufacturing using plasma technology, *Curr. Opin. Chem. Eng.*, 2022, **38**, 100857, DOI: 10.1016/j.coche.2022.100857.
80 P. J. Bruggeman, M. J. Kushner, B. R. Locke, J. G. E. Gardeniers, W. G. Graham, D. B. Graves, R. C. H. M. Hofman-Caris, D. Maric, J. P. Reid, E. Ceriani, *et al.*, Plasma–liquid interactions: a review and roadmap, *Plasma Sources Sci. Technol.*, 2016, **25**(5), 053002, DOI: 10.1088/0963-0252/25/5/053002.
81 R. Burlica, D.-E. Cretu, O. Beniuga and D. Astanei, Nonthermal Plasma Multi-Reactor Scale-Up Using Pulse Capacitive Power Supplies, *Appl. Sci.*, 2022, **12**(20), 10403.
82 Z. R. Hinton, P. A. Kots, M. Soukaseum, B. C. Vance, D. G. Vlachos, T. H. Epps and L. T. J. Korley, Antioxidant-induced transformations of a metal-acid hydrocracking catalyst in the deconstruction of polyethylene waste, *Green Chem.*, 2022, **24**(19), 7332–7339, DOI: 10.1039/D2GC02503E.
83 D. Battegazzore, S. Bocchini and A. Frache, Crystallization kinetics of poly(lactic acid)-talc composites, *eXPRESS Polym. Lett.*, 2011, **5**, 849–858, DOI: 10.3144/expresspolymlett.2011.84.
84 I. Charfeddine, J.-C. Majesté, C. Carrot and O. Lhost, Surface tension and interfacial tension of polyolefins and polyolefin blends, *J. Appl. Polym. Sci.*, 2022, **139**(14), 51885, DOI: 10.1002/app.51885.
85 G. Guerrica-Echevarría, J. I. Eguiazábal and J. Nazábal, Interfacial tension as a parameter to characterize the miscibility level of polymer blends, *Polym. Test.*, 2000, **19**(7), 849–854, DOI: 10.1016/S0142-9418(99)00055-0.
86 B. Jańczuk, W. Wójcik and A. Zdziennicka, Determination of the Components of the Surface Tension of Some Liquids from Interfacial Liquid-Liquid Tension Measurements, *J. Colloid Interface Sci.*, 1993, **157**(2), 384–393, DOI: 10.1006/jcis.1993.1200.